Ferroelectric phase transition and the lattice thermal conductivity of $Pb_{1-x}Ge_xTe$ alloys

Ronan M. Murphy,[1,2] Éamonn D. Murray,[3] Stephen Fahy,[1,2] and Ivana Savić[2,*]
[1]*Department of Physics, University College Cork, College Road, Cork, Ireland*
[2]*Tyndall National Institute, Dyke Parade, Cork, Ireland*
[3]*Department of Physics and Department of Materials, Imperial College London, London SW7 2AZ, United Kingdom*
(Received 27 December 2016; revised manuscript received 5 March 2017; published 6 April 2017)

We show how tuning the proximity to the soft optical mode phase transition via chemical composition affects the lattice thermal conductivity κ of $Pb_{1-x}Ge_xTe$ alloys. Using first-principles virtual-crystal simulations, we find that the anharmonic contribution to κ is minimized at the phase transition due to the maximized acoustic-optical anharmonic interaction. Mass disorder significantly lowers and flattens the dip in the anharmonic κ over a wide composition range, thus shifting the κ minimum away from the phase transition. The total κ and its anharmonic contribution vary continuously between the rocksalt and rhombohedral phases as expected for the second-order phase transition. The actual phase and its strength of resonant bonding play a less prominent role in reducing the κ of $Pb_{1-x}Ge_xTe$ alloys than the proximity to the phase transition and the atomic mass. Our results show that alloys with soft optical mode transitions are promising materials for achieving low thermal conductivity and possibly high thermoelectric efficiency.

DOI: 10.1103/PhysRevB.95.144302

I. INTRODUCTION

Thermoelectric materials allow for the reversible conversion of heat to electricity, which makes them particularly attractive for energy harvesting applications [1]. Nanostructuring strategies have been very successful in creating efficient thermoelectric materials by suppressing lattice thermal conductivity κ [2–7]. However, this often comes at the cost of reduced electrical conductivity and Seebeck coefficient, which results in modest increases of thermoelectric figure of merit ZT. Exploiting the fascinating properties of materials near soft mode phase transitions is an emerging alternative concept in the quest to increase ZT [8]. The underlying idea is that soft phonons strongly scatter heat-carrying acoustic modes resulting in low κ, while possibly preserving high electrical conductivity and Seebeck coefficient [9]. It has been argued that soft modes are responsible for the large ZT values of PbTe [10,11] and SnSe [8,12,13].

A number of questions need to be addressed to fully validate the concept that exceptional thermoelectric materials can be found among materials near soft mode phase transitions. One specific issue is the correlation between the lattice thermal conductivity of such materials and their proximity to the phase transition. Recent studies reported extremely low κ values in marginally stable IV-VI and I-V-VI_2 rocksalt structures [14–16]. We showed previously that driving PbTe to the verge of the phase transition to the rhombohedral phase via strain or alloying reduces the κ substantially [17]. In several I-V-VI_2 materials with slightly distorted rocksalt-like structures, κ decreases as their bond angle approaches that of the rocksalt phase [18]. Furthermore, the measured κ's of SnSe and $Pb_{1-x}Ge_xTe$ alloys exhibit pronounced dips near the transition temperatures [8,19,20]. In addition, high symmetry phases of SnSe and $AgBiSe_2$ were reported to have lower κ with respect to their distorted lower symmetry counterparts [13,15]. Similarly, first principles calculations showed that higher symmetry rocksalt IV-VI compounds have lower κ than rhombohedral group-V materials (e.g., PbTe vs Bi) [14], which was attributed to the stronger resonant bonding in the rocksalt phase [14,21,22]. These findings raise the question of whether the phase itself plays a key role in suppressing κ alongside the proximity to a soft mode phase transition. Furthermore, it is not known how the interplay of alloy disorder, structure, and soft modes will affect the κ of alloys with soft mode transitions, such as $Pb_{1-x}Ge_xTe$.

In this paper, we investigate the impact of proximity to the ferroelectric phase transition on the lattice thermal conductivity of $Pb_{1-x}Ge_xTe$ alloys by tuning their composition. These alloys undergo a soft optical mode transition between the rocksalt and rhombohedral phases as a function of the composition and temperature [23], and have high ZT [19,20,24–27]. Our first principles virtual-crystal calculations show that the phase transition minimizes the anharmonic component of κ due to extremely soft optical modes which maximize the anharmonic acoustic-optical coupling, especially for low-frequency phonons. Mass disorder additionally reduces κ via scattering of mid- and high frequencies, which flattens the drop in the anharmonic κ over a wide range of compositions and moves the κ minimum away from the phase transition. Furthermore, we find a continuous change of the total and anharmonic κ between the rocksalt and rhombohedral phases characteristic of the second-order phase transition. We argue that the structure and its degree of resonant bonding are less crucial for lowering the κ in these alloys than the proximity to the phase transition, average atomic mass, and mass disorder. Our findings highlight the potential of combining soft optical modes and alloying to design materials with low κ and potentially high ZT.

II. METHODOLOGY

We compute the lattice thermal conductivity of $Pb_{1-x}Ge_xTe$ alloys from first principles, combining density functional theory (DFT) [28] and the Boltzmann transport equation in the relaxation time approximation (BTE-RTA) [29]. This

*ivana.savic@tyndall.ie

approach typically gives κ values in good agreement with experiment [11,30–33], and can be used to predict the κ of proposed new materials. The lattice thermal conductivity (for simplicity thermal conductivity from here on) is given by [29]

$$\kappa = \frac{1}{NV}\sum_{\mathbf{q},s} c_{\mathbf{q},s} v^2_{\mathbf{q},s} \tau_{\mathbf{q},s}, \quad (1)$$

where ($\mathbf{q}$,s) denotes the wave vector $\mathbf{q}$ and branch index s of a phonon mode with frequency $\omega_{\mathbf{q},s}$. $c_{\mathbf{q},s}$ is the heat capacity, $v_{\mathbf{q},s} = \mathrm{d}\omega_{\mathbf{q},s}/\mathrm{d}\mathbf{q}$ the group velocity, and $\tau_{\mathbf{q},s}$ the phonon lifetime. V is the primitive cell volume and N is the total number of sampled $\mathbf{q}$ points. We use $20 \times 20 \times 20$ grids in the Brillouin zone for the κ calculations (we verified that using $40 \times 40 \times 40$ grids changes the κ values by no more than a few percent with respect to $20 \times 20 \times 20$ grids). Anharmonic phonon lifetimes are calculated taking into account the contribution of three-phonon scattering processes [29,34,35]. $Pb_{1-x}Ge_xTe$ alloys are treated using the virtual crystal approximation, thus assuming a displacive second-order phase transition [36,37]. Mass disorder is modeled via an effective phonon lifetime given as [38,39]

$$\tau^{-1}_{\mathbf{q},s} = \frac{\pi}{2N}\omega^2_{\mathbf{q},s}\sum_{\mathbf{q}',s'}\delta(\omega_{\mathbf{q},s} - \omega_{\mathbf{q}',s'}) \times \sum_{\sigma} g(\sigma)|\mathbf{e}^*_{\mathbf{q},s}(\sigma)\cdot\mathbf{e}_{\mathbf{q},s}(\sigma)|^2, \quad (2)$$

where $\mathbf{e}_{\mathbf{q},s}$ is the eigenvector of mode ($\mathbf{q}$,s). The strength of mass disorder is defined as $g(\sigma) = \sum_i f_i(\sigma)[1 - m_i(\sigma)/\bar{m}_i(\sigma)]^2$, where $f_i(\sigma)$ and $m_i(\sigma)$ are the fraction and the atomic mass of the ith atomic species occupying atom σ in the virtual crystal lattice, while $\bar{m}_i(\sigma)$ is its average mass. We calculate κ combining the phonon lifetimes due to mass disorder with the anharmonic (three-phonon) lifetimes using Mattheisen's rule. Disorder in the force constants is not treated in our approach, and its inclusion would only increase the κ reductions predicted here [40].

The real-space finite difference supercell approach [31] as implemented in the PHONO3PY code [41,42] is used to calculate harmonic and anharmonic interactomic force constants (IFCs) at zero temperature from the Hellmann-Feynman forces. Forces are computed on $4 \times 4 \times 4$ (128 atom) supercells (see Supplemental Material [43]) with an energy cutoff of 15 Ha. DFT calculations are performed with the ABINIT code [44], using the local density approximation for the exchange correlation functional and Hartwigsen-Goedecker-Hutter norm-conserving pseudopotentials [45]. Electronic states are described using four shifted $2 \times 2 \times 2$ fcc Brillouin zone grids for alloy compositions $x \leqslant 0.51$, while $2 \times 2 \times 2$ rhombohedral Brillouin zone grids are used for all other compositions. Born effective charges and dielectric permittivity tensors are calculated using density functional perturbation theory, as implemented in ABINIT [44,46,47].

The described method, however, does not account for the temperature dependence of structural parameters and IFCs. As a result, we do not capture the phase transition in $Pb_{1-x}Ge_xTe$ alloys from the rhombohedral to rocksalt phases with increasing temperature at a given composition [23]. The temperature at which the phase transition occurs increases as a function of Ge content, from 0 K at $x \approx 0.01$ to ~670 K for $x = 1$ [23]. Nonetheless, we find that the phonon dispersions, thermal expansion coefficients, and κ of PbTe and GeTe agree fairly well with experimental data (see Supplemental Material [48]). Furthermore, our model captures the soft optical mode phase transition as a function of the alloy composition, as we will show in the next section. This suggests that our approach will correctly predict qualitative changes in the κ of $Pb_{1-x}Ge_xTe$ alloys by varying x.

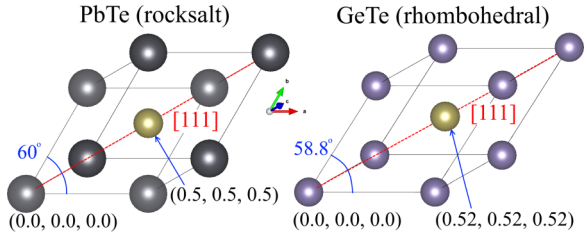

FIG. 1. Rocksalt and rhombohedral structures of PbTe and GeTe, respectively. The differences between the two structures are the position of Te atom along the trigonal [111] axis and the angle between the primitive lattice vectors. The rocksalt phase is a special case of the rhombohedral phase with the relative Te position of (0.5,0.5,0.5) within the primitive cell, and the angle of 60°.

III. $Pb_{1-x}Ge_xTe$ ALLOYS AND THE FERROELECTRIC PHASE TRANSITION

PbTe crystallizes in the rocksalt structure, while GeTe forms a rhombohedral structure, shown in Fig. 1. The relative positions of Pb and Te atoms within the rocksalt primitive cell are (0,0,0) and (0.5,0.5,0.5), and the angle between the lattice vectors is $\phi = 60°$. In the rhombohedral lattice, the relative position of the second atom is $(0.5 + r, 0.5 + r, 0.5 + r)$, and the angle is $\phi = 60° - \theta$. Consequently, the rhombohedral lattice has a trigonal symmetry with respect to the [111] direction. In GeTe, the relative Te position is (0.52,0.52,0.52), and the angle is $\phi = 58.8°$ [71,72]. The rocksalt phase is a special case of the rhombohedral phase with $r = 0$ and $\theta = 0°$ (see Supplemental Material [48] for further discussion). By varying the alloy composition, $Pb_xGe_{1-x}Te$ alloys will undergo a second order phase transition between the rocksalt and rhombohedral phases. A typical feature of the second order phase transition is a continuous change of the values of various physical quantities at the phase transition (e.g., see the continuous change in lattice parameters of $Pb_xGe_{1-x}Te$ as a function of x in Supplemental Material [48]).

We illustrate the alloy composition at which the phase transition occurs within our model by plotting the frequency of the lowest transverse optical mode at Γ, TO(Γ), as a function of x; see Fig. 2. The phase transition takes place for $x = 0.492$, when the frequency of TO(Γ) becomes ≈0 THz. For $0 \leqslant x < 0.492$, the rocksalt structure is energetically preferable, and the TO(Γ) frequency decreases smoothly with increasing x, from ~1.0 THz in PbTe to ~0.2 THz for $x = 0.49$. The rhombohedral structure is favorable for $0.492 < x \leqslant 1$, and the TO(Γ) frequency decreases almost linearly with decreasing x, from ~2.0 THz in GeTe to ~0.4 THz at $x = 0.51$. In the immediate vicinity of the structural transition, the TO(Γ)

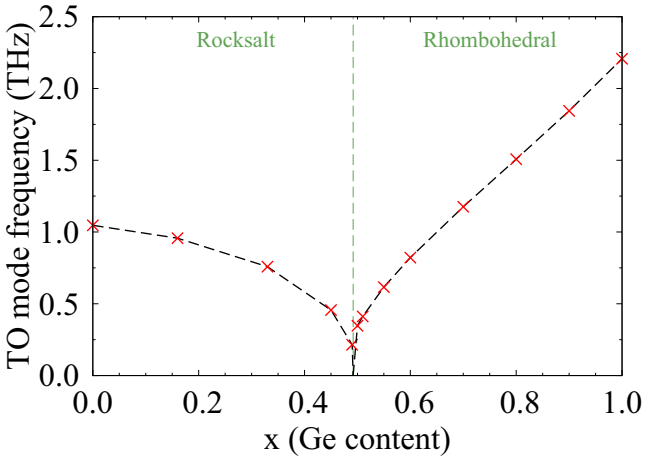

FIG. 2. Frequency of the lowest transverse optical mode at the zone center, TO(Γ), as a function of $Pb_{1-x}Ge_xTe$ alloy composition.

frequency is higher in the rhombohedral phase compared to the rocksalt phase by a factor of $\sim\sqrt{2}$ (for $x = 0.491$ and $x = 0.493$, respectively). This value can also be obtained analytically by examining the total energy as a function of the TO atomic displacement for the two phases (see Supplemental Material [48]). We note that since the transition temperature of $Pb_{0.5}Ge_{0.5}Te$ is ∼450 K [23], our model best describes the soft TO modes and κ of $Pb_{1-x}Ge_xTe$ alloys near this temperature.

In addition to dramatic softening of TO(Γ) modes, we illustrate the full impact of increased proximity to the phase transition on the phonon dispersions of $Pb_{1-x}Ge_xTe$ alloys. Figure 3(a) compares the phonon dispersions of two rhombohedral structures: GeTe and a composition on the verge of the phase transition, $Pb_{0.49}Ge_{0.51}Te$. Similarly, in the rocksalt phase we compare PbTe and $Pb_{0.51}Ge_{0.49}Te$; see Fig. 3(b). Away from the zone center, phonon frequencies become significantly lower as the value of x decreases in both the rocksalt and rhombohedral phases. This change is largely due to the heavier average atomic mass as the alloy composition varies from GeTe to PbTe. At the phase transition, the phonon dispersions of the rocksalt and rhombohedral structures are remarkably similar; see Fig. 3(c). This is due to the fact that the soft optical mode transition in $Pb_{1-x}Ge_xTe$ alloys is second order.

IV. PHONON LIFETIMES

The extremely soft TO modes at the ferroelectric phase transition minimize the anharmonic phonon lifetimes of $Pb_{1-x}Ge_xTe$ alloys in both the rocksalt and rhombohedral phases. In the rhombohedral phase, three-phonon lifetimes are reduced by a factor of ∼2 in $Pb_{0.49}Ge_{0.51}Te$ compared to GeTe at 450 K [Fig. 4(a)]. This reduction is maintained across the entire frequency spectrum, which is more clearly shown in the inset of Fig. 4(a), where averaged anharmonic lifetimes, defined as $\langle\tau\rangle = \sum_{\mathbf{q},s}\tau_{\mathbf{q},s}\delta(\omega-\omega_{\mathbf{q},s})/\sum_{\mathbf{q},s}\delta(\omega-\omega_{\mathbf{q},s})$, are plotted versus frequency. In the rocksalt phase, anharmonic lifetimes τ are also minimized at the phase transition, as illustrated by their comparison for $Pb_{0.51}Ge_{0.49}Te$ and PbTe in Fig. 4(b). However, in this case the reduction is mainly

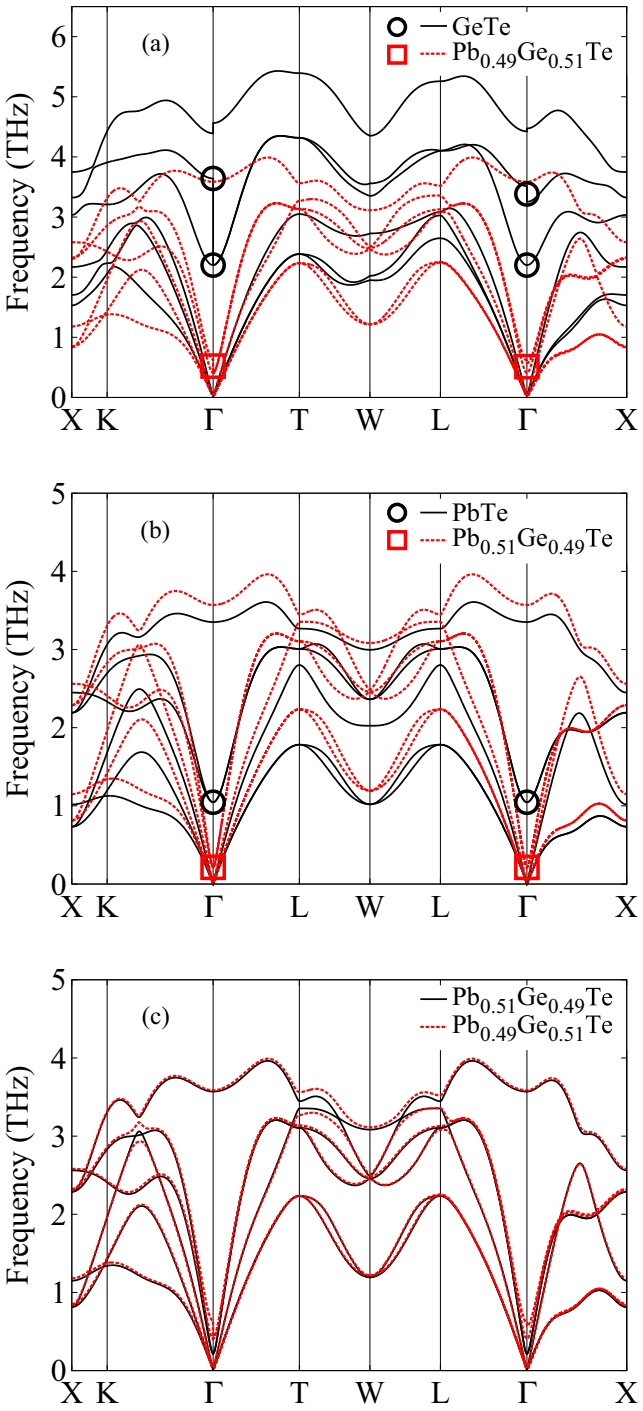

FIG. 3. (a) Phonon band structures at 0 K for GeTe (solid black line) and an alloy in the rhombohedral structure near the phase transition, $Pb_{0.49}Ge_{0.51}Te$ (dashed red line). The frequencies of the soft transverse optical phonon modes at the zone center, TO(Γ), are highlighted in black circles for GeTe and red squares for $Pb_{0.49}Ge_{0.51}Te$. (b) Phonon band structures at 0 K for PbTe (solid black line) and an alloy in the rocksalt structure near the phase transition, $Pb_{0.51}Ge_{0.49}Te$ (dashed red line). TO(Γ) mode frequencies are highlighted in black circles for PbTe and red squares for $Pb_{0.51}Ge_{0.49}Te$. (c) Phonon band structures at 0 K for alloy compositions in the rocksalt and rhombohedral phases near the phase transition: $Pb_{0.51}Ge_{0.49}Te$ (solid black line) and $Pb_{0.49}Ge_{0.51}Te$ (dashed red line), respectively.

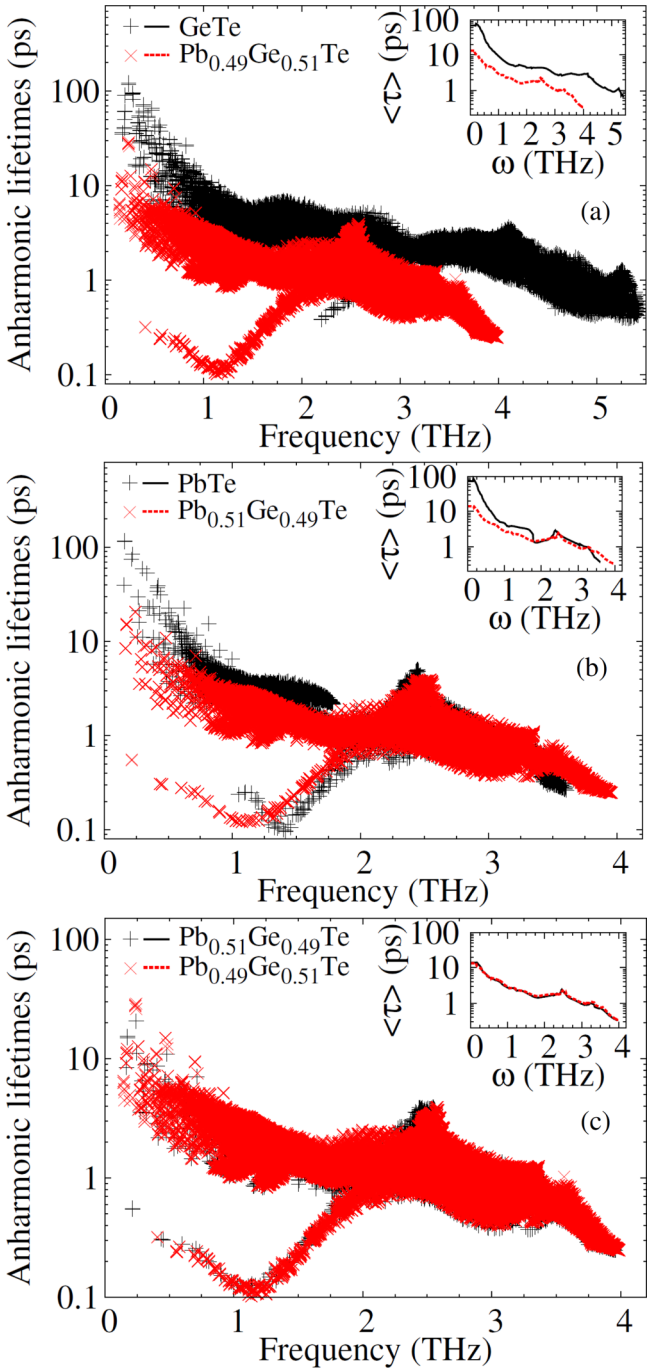

FIG. 4. (a) Anharmonic (three-phonon) phonon lifetimes at 450 K as a function of frequency for GeTe (black pluses) and a rhombohedral alloy near the phase transition, $Pb_{0.49}Ge_{0.51}Te$ (red crosses). Inset: averaged anharmonic lifetimes vs frequency at 450 K for GeTe (solid black line) and $Pb_{0.49}Ge_{0.51}Te$ (dashed red line). (b) Anharmonic lifetimes at 450 K as a function of frequency for PbTe (black pluses) and a rocksalt alloy near the phase transition, $Pb_{0.51}Ge_{0.49}Te$ (red crosses). Inset: averaged lifetimes vs frequency at 450 K for GeTe (solid black line) and $Pb_{0.51}Ge_{0.49}Te$ (dashed red line). (c) Anharmonic lifetimes at 450 K as a function of frequency for rocksalt $Pb_{0.51}Ge_{0.49}Te$ (black pluses) and rhombohedral $Pb_{0.49}Ge_{0.51}Te$ (red crosses). Inset: averaged lifetimes vs frequency at 450 K for $Pb_{0.51}Ge_{0.49}Te$ (solid black line) and $Pb_{0.49}Ge_{0.51}Te$ (dashed red line).

concentrated to lower frequencies. The significant decrease of anharmonic τ at the phase transition offers new alternatives in the search for techniques to suppress lifetimes across the frequency spectrum. Furthermore, the anharmonic τ of the rocksalt and rhombohedral structures in the vicinity of the phase transition are very similar [Fig. 4(c)]. This similarity is a direct result of the second-order phase transition, and results in the continuous change of anharmonic lifetimes as the alloy composition is varied.

The maximal softening of the TO mode at the zone center is directly responsible for the maximal strength of the anharmonic coupling of TO modes with heat-carrying acoustic modes, and the minimization of anharmonic lifetimes at the phase transition. We computed the acoustic-TO contribution to the lifetimes at all frequencies by accounting for the triplets of interacting states that contain at least one acoustic and one TO mode as described in Ref. [17]. We distinguished between TO and longitudinal acoustic (LA) modes whose order changes throughout the Brillouin zone by projecting their eigenvectors onto the corresponding wave vector, and then determined which state is more longitudinal. We found that the acoustic-TO contribution to the lifetime dominates over the other contributions across the spectrum, and becomes maximal at the phase transition (see Supplemental Material [48]).

The effect of mass disorder on phonon lifetimes in $Pb_{1-x}Ge_xTe$ alloys is strongest for $x \approx 0.6$. By taking the derivative of the expression for the mass disorder strength g on the Pb/Ge site, it can be derived that g reaches a maximum for $x = m_{Pb}/(m_{Ge} + m_{Pb}) = 0.74$. Nevertheless, the larger density of states for compositions with smaller Ge content shifts the composition at which the overall scattering due to mass disorder is strongest to $x \approx 0.6$. Mass disorder is more effective at scattering mid- and high-frequency phonons in comparison to anharmonic processes. However, at low frequencies, anharmonic τ are smaller than those due to mass disorder by several orders of magnitude (see Supplemental Material [48]). This highlights the effectiveness of the strategy of combining soft modes and alloying to design materials with low thermal conductivity.

V. THERMAL CONDUCTIVITY

The ferroelectric phase transition minimizes the anharmonic contribution to the thermal conductivity of $Pb_{1-x}Ge_xTe$ alloys in both the rocksalt and rhombohedral phases. This is shown by the unfilled symbols in Fig. 5, which represent the anharmonic κ as a function of x at 450 K. In the rhombohedral phase, the anharmonic κ of the composition very near the phase transition, $x = 0.51$, decreases by a factor of $\sim$2.4 ($\sim$1.8) in the direction perpendicular (parallel) to the trigonal [111] axis with respect to GeTe. These reductions are a direct result of the substantial decrease in the anharmonic τ of $Pb_{0.49}Ge_{0.51}Te$ [see Fig. 4(a)], and are further enhanced by its lower group velocities due to the heavier average atomic mass. The anisotropy in the anharmonic κ of the rhombohedral structures decreases from $\sim$29% in GeTe towards zero at the phase transition. In the rocksalt phase, the anharmonic κ initially slightly increases for low values of x, and then decreases as x becomes larger. This effect is due to the larger

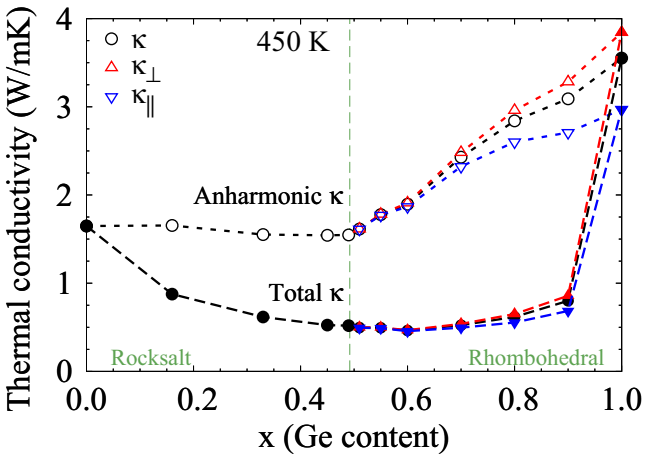

FIG. 5. Lattice thermal conductivity of $Pb_{1-x}Ge_xTe$ as a function of the alloy composition at 450 K. The unfilled symbols show the thermal conductivity due to anharmonic (three-phonon) processes only, and the filled symbols show the thermal conductivity due to anharmonic processes and mass disorder. Black circles show the thermal conductivity in the rocksalt phase and its isotropic average in the rhombohedral phase. Red up and blue down triangles show the thermal conductivity perpendicular and parallel to the trigonal [111] axis in the rhombohedral phase, respectively.

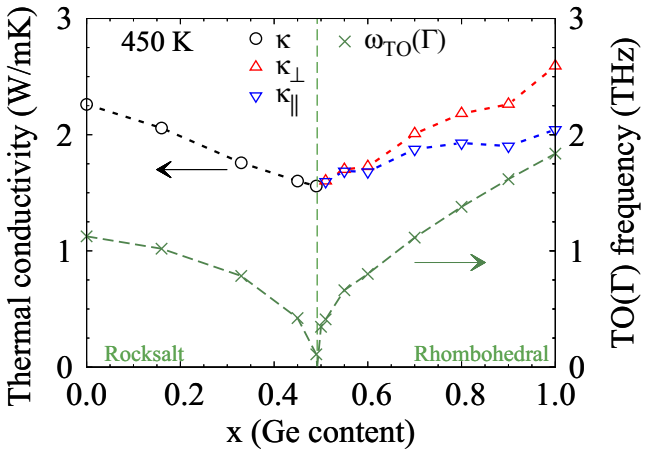

FIG. 6. Anharmonic contribution to the lattice thermal conductivity of $Pb_{1-x}Ge_xTe$ as a function of the alloy composition at 450 K, where the group IV element mass of each alloy composition is artificially set to that of $Pb_{0.5}Ge_{0.5}Te$. Black circles show the thermal conductivity in the rocksalt phase, while red up and blue down triangles show the thermal conductivity perpendicular and parallel to the trigonal [111] axis in the rhombohedral phase, respectively. Also shown in green crosses is the frequency of the lowest transverse optical mode at the zone center for the same mass of the group IV element as described above.

group velocities competing with the reduced phonon lifetimes as the proximity to the phase transition is increased with x. Overall, there is a modest reduction by a factor of ~1.05 in the anharmonic κ at $x = 0.49$ with respect to that of PbTe. This results in the asymmetric reductions of the anharmonic κ for the rocksalt and rhombohedral phases (see Fig. 5). Importantly, the anharmonic κ changes continuously as the alloy undergoes the second-order phase transition as a result of the continuous variation of phonon lifetimes and group velocities.

Neglecting the average mass difference among $Pb_{1-x}Ge_xTe$ compositions removes the asymmetric reductions in the anharmonic thermal conductivity for the two phases, and further highlights its minimization at the phase transition. This is illustrated in Fig. 6, where the mass difference is ignored by artificially setting the group IV element mass of each alloy composition to that of $Pb_{0.5}Ge_{0.5}Te$. The anharmonic κ decreases smoothly with the increased proximity to the phase transition mostly due to the reduced anharmonic τ, which results in a factor of ~1.5 reduction in both the rocksalt and rhombohedral phases with respect to $x = 0$ and 1. Therefore, the minimization of anharmonic κ at the phase transition would be more pronounced for alloys with soft optical modes whose overall mass difference is smaller than that of $Pb_{1-x}Ge_xTe$ alloys, or for bulk materials driven to the phase transition via pressure or strain [17]. However, the κ of such materials may not be as low as reported here since mass disorder would be irrelevant or weaker than in $Pb_{1-x}Ge_xTe$.

Mass disorder significantly reduces the thermal conductivity of $Pb_{1-x}Ge_xTe$ alloys, thereby flattening the dip in its anharmonic contribution and shifting the minimum away from the phase transition (Fig. 5). The minimal κ occurs at $x \approx 0.6$ in our model where the overall scattering due to mass disorder is maximized, and near the composition where the phase transition occurs ($x = 0.5$). Our results illustrate a general trend that the minimal κ in alloys with soft optical modes will be determined by the interplay among anharmonicity, average mass, and mass disorder, and it will not necessarily occur at the phase transition. We find the factors of ~7.7 and ~3.6 reduction in the isotropically averaged κ at its minimal value at 450 K with respect to GeTe and PbTe, respectively. Interestingly, for the alloy composition of $x = 0.9$, scattering due to mass disorder is relatively strong at high frequencies due to the high density of states, resulting in the κ value which is comparable to the κ minimum at $x \approx 0.6$. We note that disorder in the force constants would further suppress the thermal conductivity values reported here [40].

VI. IMPACT OF STRUCTURE AND RESONANT BONDING

If the overall mass difference in $Pb_{1-x}Ge_xTe$ alloys could be ignored, the anharmonic thermal conductivity would be comparably suppressed in the rocksalt and rhombohedral structures with the similar proximity to the phase transition. This is shown in Fig. 6, where the dependence of the anharmonic κ on x is compared with that of the TO(Γ) frequency when the group IV element mass of each alloy composition is set to that of $Pb_{0.5}Ge_{0.5}Te$. Here we consider TO(Γ) frequency as a rough measure of the proximity to the phase transition of both rocksalt and rhombohedral phases. The anharmonic κ of a rhombohedral structure is comparable to that of the rocksalt structure with a similar TO(Γ) frequency, and it is even notably lower in the direction parallel to the trigonal axis. This is in contrast with the previous reports that high symmetry phases have lower κ compared to their lower symmetry counterparts [13–15]. However, these studies did not attempt to tune the proximity to the phase transition of these materials to fully investigate this effect. Our analysis suggests

that the proximity to the phase transition, average atomic mass, and mass disorder are more dominant mechanisms for the thermal conductivity reduction in $Pb_{1-x}Ge_xTe$ alloys than the symmetry of the phase.

Our findings are in partial disagreement with the recent claims that stronger resonant bonding leads to lower thermal conductivity in rocksalt IV-VI and rhombohedral group-V materials [14]. Resonant bonding is characterized by half-saturated p-bonds typical for these materials, which results in delocalized electron densities and large electronic polarizabilities [14,21,66] (see Born effective charges and dielectric constants of $Pb_{1-x}Ge_xTe$ versus x in Supplemental Material [48]). This leads to large values of the harmonic IFCs for the fourth and eighth nearest neighbors (NNs) [14,73], which correspond to the second and third NNs along the [001] direction in the rocksalt structure, respectively [see Fig. 7(a)]. It has been argued that the larger the magnitude of these long-range IFCs (i.e., the stronger the degree of resonant bonding), the softer the TO mode and lower the κ of these materials [14].

We find that the long-range harmonic IFCs along the [001] direction in $Pb_{1-x}Ge_xTe$ alloys are indeed maximized at the phase transition where the thermal conductivity is minimized. The traces of the harmonic IFC tensors for several different alloy compositions are shown in Figs. 7(b) and 7(c) for the rhombohedral and rocksalt phases, respectively. In both phases, we see particularly strong IFCs at ~3 Å, ~6 Å, and ~9 Å, which correspond to the first, fourth, and eighth NNs in the rocksalt structure, respectively, and their rhombohedral equivalents. IFCs change continuously between the rocksalt and rhombohedral phases as a consequence of the second-order phase transition. This can be seen by comparing the IFCs of $Pb_{0.49}Ge_{0.51}Te$ with those of $Pb_{0.51}Ge_{0.49}Te$, as shown in Fig. 7(b). As proximity to the phase transition increases, the magnitudes of the fourth and eighth equivalent neighbor IFCs increase substantially and reach maximum values at the phase transition. As discussed earlier, the TO(Γ) frequency reaches its minimal value at the phase transition, and the maximized anharmonic coupling between soft TO and acoustic modes results in the minimal κ. Thus we observe the correlation between the large long-range IFCs along the [001] direction and the substantially reduced κ as proposed in Ref. [14].

However, in spite of weaker resonant bonds, the anharmonic thermal conductivity values of the rhombohedral structures are as low as for the rocksalt structures with a similar proximity to the phase transition when their average mass difference is neglected. The short-range IFCs which correspond to the first NN increase rapidly in the rhombohedral phase with increasing x with respect to the fourth and eighth IFCs, as shown in Fig. 7(b). The relative change between the short-range and the long-range IFCs is much smaller in the rocksalt than in the rhombohedral phase, which indicates much weaker resonant bonding in the rhombohedral structures due to the Te displacement. This stark difference in the strength of resonant bonding between the two phases does not result in larger values of the anharmonic κ of rhombohedral structures compared to rocksalt structures with the same average mass (Fig. 6). This conclusion is at variance with the previous argument that stronger resonant bonding causes lower thermal conductivity in rocksalt IV-VI and rhombohedral group-V materials [14].

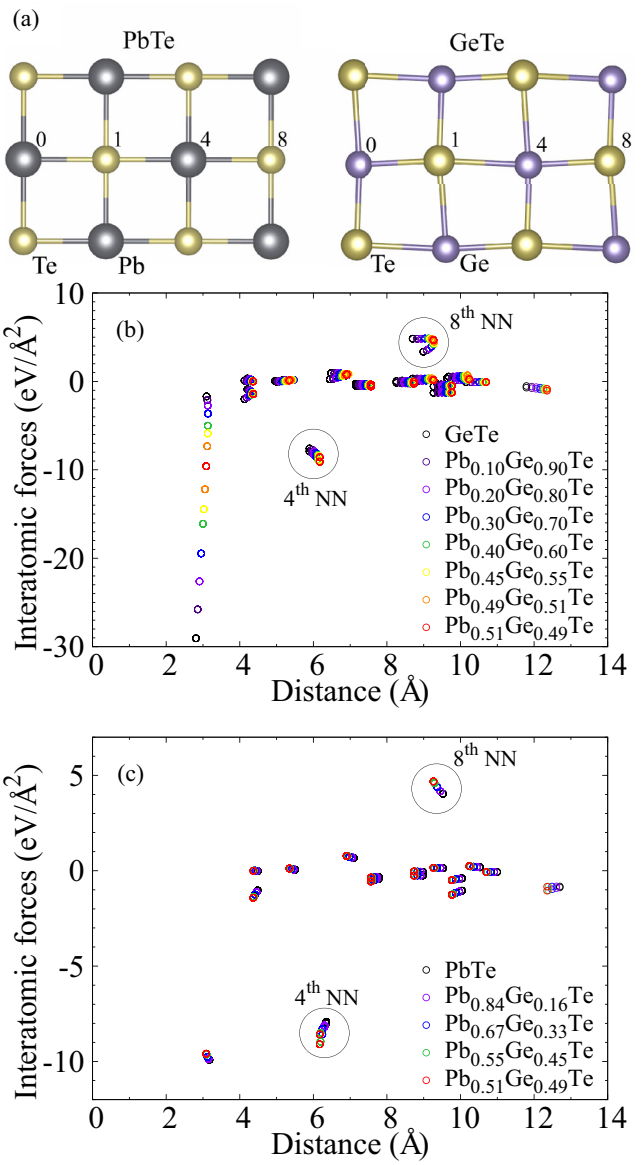

FIG. 7. (a) Nearest neighbors within the rocksalt structure of PbTe along the [001] direction, and their counterparts for the rhombohedral structure of GeTe. (b) The trace of the harmonic interatomic force constant tensor vs atomic distance for several $Pb_{1-x}Ge_xTe$ alloy compositions in the rhombohedral phase. An alloy composition in the rocksalt phase near the phase transition, $Pb_{0.51}Ge_{0.49}Te$, is also included for comparison. (c) The trace of the harmonic interatomic force constant tensor vs atomic distance for several $Pb_{1-x}Ge_xTe$ alloy compositions in the rocksalt phase.

VII. DISCUSSION

There has been a recent debate in the literature whether PbTe crystallizes in the ideal rocksalt structure [74–77], or forms local structural dipoles with increasing temperature [78–81]. Another controversial issue is whether $Pb_{1-x}Ge_xTe$ alloys undergo a displacive second-order [36,37] or an order-disorder [50,59,82,83] phase transition with composition and temperature. Resolving these questions is beyond the scope of this work. Here we assume that PbTe has the rocksalt

structure, and that $Pb_{1-x}Ge_xTe$ alloys go through a displacive second-order phase transition as a function of x.

Under the assumption of the displacive second-order phase transition, $Pb_{1-x}Ge_xTe$ alloys transform between the rocksalt and rhombohedral phases as a function of both the composition and temperature. Consequently, the anharmonic contribution to the lattice thermal conductivity of $Pb_{1-x}Ge_xTe$ will be minimized at different compositions as a function of temperature. Similarly, the anharmonic lattice thermal conductivity for a given x will have a dip in the vicinity of the corresponding transition temperature. The accurate treatment of these effects would require extending our model to include the temperature dependence of IFCs as done, e.g., in Refs. [64,84]. Additionally, the electrical thermal conductivity will be significant in Ge-rich alloys due to a large intrinsic vacancy concentration that effectively dopes the material [60,65].

VIII. CONCLUSION

We predict from first principles virtual-crystal simulations that the anharmonic contribution to the lattice thermal conductivity of $Pb_{1-x}Ge_xTe$ alloys is minimized at the soft optical mode phase transition due to the maximized acoustic-optical anharmonic interaction. The total lattice thermal conductivity is further considerably reduced due to mass disorder, which shifts the minimum value away from the phase transition. The total lattice thermal conductivity and its anharmonic component change continuously between the rocksalt and rhombohedral phases of the alloy as typical for the second-order phase transition. We argue that the structure and its degree of resonant bonding are less critical factors for the low thermal conductivity than the proximity to the phase transition, average atomic mass, and mass disorder. Due to the symmetry-forbidden electron-phonon coupling between the TO mode at Γ and the valence band maximum and conduction band minimum in PbTe [17,85], the electronic properties beneficial for a high figure of merit may not be hindered by the phase transition. Consequently, combining soft optical modes with alloying is a promising strategy in the design of materials with low thermal conductivity and high thermoelectric figure of merit.

ACKNOWLEDGMENTS

This work was supported by Science Foundation Ireland (SFI) and the Marie-Curie Action COFUND under Starting Investigator Research Grant No. 11/SIRG/E2113, and by SFI and Department of Education and Learning, Northern Ireland under Investigators Programme No. 15/1A/3160. We acknowledge the Irish Centre for High-End Computing (ICHEC) for the provision of computational facilities. We thank Yaniv Gelbstein and Mike Finnis for useful discussions.

[1] G. D. Mahan, APL Mater. **4**, 104806 (2016).
[2] G. Tan, L.-D. Zhao, and M. G. Kanatzidis, Chem. Rev. **116**, 12123 (2016).
[3] D. G. Cahill, P. V. Braun, G. Chen, D. R. Clarke, S. Fan, K. E. Goodson, P. Keblinski, W. P. King, G. D. Mahan, A. Majumdar, H. J. Maris, S. R. Phillpot, E. Pop, and L. Shi, Appl. Phys. Rev. **1**, 011305 (2014).
[4] J. P. Heremans, M. S. Dresselhaus, L. E. Bell, and D. T. Morelli, Nat. Nanotechnol. **8**, 471 (2013).
[5] K. Biswas, J. He, I. D. Blum, C.-I. Wu, T. P. Hogan, D. N. Seidman, V. P. Dravid, and M. G. Kanatzidis, Nature (London) **489**, 414 (2012).
[6] C. J. Vineis, A. Shakouri, A. Majumdar, and M. G. Kanatzidis, Adv. Mater. **22**, 3970 (2010).
[7] G. J. Snyder and E. S. Toberer, Nat. Mater. **7**, 105 (2008).
[8] L.-D. Zhao, S.-H. Lo, Y. Zhang, H. Sun, G. Tan, C. Uher, C. Wolverton, V. P. Dravid, and M. G. Kanatzidis, Nature (London) **508**, 373 (2014).
[9] L.-D. Zhao, G. Tan, S. Hao, J. He, Y. Pei, H. Chi, H. Wang, S. Gong, H. Xu, V. P. Dravid, C. Uher, G. J. Snyder, C. Wolverton, and M. G. Kanatzidis, Science **351**, 141 (2016).
[10] O. Delaire, J. Ma, K. Marty, A. F. May, M. A. McGuire, M.-H. Du, D. J. Singh, A. Podlesnyak, G. Ehlers, M. D. Lumsden, and B. C. Sales, Nat. Mater. **10**, 614 (2011).
[11] T. Shiga, J. Shiomi, J. Ma, O. Delaire, T. Radzynski, A. Lusakowski, K. Esfarjani, and G. Chen, Phys. Rev. B **85**, 155203 (2012).
[12] C. W. Li, J. Hong, A. F. May, D. Bansal, S. Chi, T. Hong, G. Ehlers, and O. Delaire, Nat. Phys. **11**, 1063 (2015).
[13] J. M. Skelton, L. A. Burton, S. C. Parker, A. Walsh, C.-E. Kim, A. Soon, J. Buckeridge, A. A. Sokol, C. R. A. Catlow, A. Togo, and I. Tanaka, Phys. Rev. Lett. **117**, 075502 (2016).
[14] S. Lee, K. Esfarjani, T. Luo, J. Zhou, Z. Tian, and G. Chen, Nat. Commun. **5**, 3525 (2014).
[15] M. D. Nielsen, V. Ozolins, and J. P. Heremans, Energy Environ. Sci. **6**, 570 (2013).
[16] D. T. Morelli, V. Jovovic, and J. P. Heremans, Phys. Rev. Lett. **101**, 035901 (2008).
[17] R. M. Murphy, E. D. Murray, S. Fahy, and I. Savić, Phys. Rev. B **93**, 104304 (2016).
[18] E. J. Skoug and D. T. Morelli, Phys. Rev. Lett. **107**, 235901 (2011).
[19] Z. Lu, J. Li, C. Wang, Y. Li, F. Liu, and W. Ao, J. Alloys Compd. **621**, 345 (2015).
[20] Y. Gelbstein and J. Davidow, Phys. Chem. Chem. Phys. **16**, 20120 (2014).
[21] G. Lucovsky and R. M. White, Phys. Rev. B **8**, 660 (1973).
[22] K. Shportko, S. Kremers, M. Woda, D. Lencer, J. Robertson, and M. Wuttig, Nat. Mater. **7**, 653 (2008).
[23] D. K. Hohnke, H. Holloway, and S. Kaiser, J. Phys. Chem. Solids **33**, 2053 (1972).
[24] S. Perumal, S. Roychowdhury, and K. Biswas, J. Mater. Chem. C **4**, 7520 (2016).
[25] D. Wu, L.-D. Zhao, S. Hao, Q. Jiang, F. Zheng, J. W. Doak, H. Wu, H. Chi, Y. Gelbstein, C. Uher, C. Wolverton, M. Kanatzidis, and J. He, J. Am. Chem. Soc. **136**, 11412 (2014).
[26] Y. Gelbstein, J. Davidow, S. N. Girard, D. Y. Chung, and M. Kanatzidis, Adv. Energy Mat. **3**, 815 (2013).
[27] S. Li, J. Li, Q. Wang, L. Wang, F. Liu, and W. Ao, Solid State Sci. **13**, 399 (2011).
[28] M. C. Payne, M. P. Teter, D. C. Allan, T. A. Arias, and J. D. Joannopoulos, Rev. Mod. Phys. **64**, 1045 (1992).
[29] G. P. Srivastava, *The Physics of Phonons* (Taylor & Francis Group, New York, 1990).

[30] D. A. Broido, M. Malorny, G. Birner, N. Mingo, and D. A. Stewart, Appl. Phys. Lett. **91**, 231922 (2007).

[31] K. Esfarjani, G. Chen, and H. T. Stokes, Phys. Rev. B **84**, 085204 (2011).

[32] J. Garg, N. Bonini, B. Kozinsky, and N. Marzari, Phys. Rev. Lett. **106**, 045901 (2011).

[33] L. Lindsay, D. A. Broido, and T. L. Reinecke, Phys. Rev. B **87**, 165201 (2013).

[34] I. Savić, D. Donadio, F. Gygi, and G. Galli, Appl. Phys. Lett. **102**, 073113 (2013).

[35] Y. He, I. Savić, D. Donadio, and G. Galli, Phys. Chem. Chem. Phys. **14**, 16209 (2012).

[36] T. Chattopadhyay, J. X. Boucherle, and H. G. von Schnering, J. Phys. C **20**, 1431 (1987).

[37] U. D. Wdowik, K. Parlinski, S. Rols, and T. Chatterji, Phys. Rev. B **89**, 224306 (2014).

[38] Z. Tian, J. Garg, K. Esfarjani, T. Shiga, J. Shiomi, and G. Chen, Phys. Rev. B **85**, 184303 (2012).

[39] S.-i. Tamura, Phys. Rev. B **27**, 858 (1983).

[40] P. G. Klemens, Proc. Phys. Soc. London, Sect. A **68**, 1113 (1955).

[41] A. Togo, F. Oba, and I. Tanaka, Phys. Rev. B **78**, 134106 (2008).

[42] A. Togo, L. Chaput, I. Tanaka, and G. Hug, Phys. Rev. B **81**, 174301 (2010).

[43] See Supplemental Material at http://link.aps.org/supplemental/10.1103/PhysRevB.95.144302 for more details about our choice of supercell size.

[44] X. Gonze, B. Amadon, P.-M. Anglade, J.-M. Beuken, F. Bottin, P. Boulanger, F. Bruneval, D. Caliste, R. Caracas, M. Cote, T. Deutsch, L. Genovese, P. Ghosez, M. Giantomassi, S. Goedecker, D. Hamann, P. Hermet, F. Jollet, G. Jomard, S. Leroux, M. Mancini, S. Mazevet, M. Oliveira, G. Onida, Y. Pouillon, T. Rangel, G.-M. Rignanese, D. Sangalli, R. Shaltaf, M. Torrent, M. Verstraete, G. Zerah, and J. Zwanziger, Comput. Phys. Commun. **180**, 2582 (2009).

[45] C. Hartwigsen, S. Goedecker, and J. Hutter, Phys. Rev. B **58**, 3641 (1998).

[46] X. Gonze, Phys. Rev. B **55**, 10337 (1997).

[47] X. Gonze and C. Lee, Phys. Rev. B **55**, 10355 (1997).

[48] See Supplemental Material at http://link.aps.org/supplemental/10.1103/PhysRevB.95.144302 for a more detailed discussion and the figures of some of the effects discussed in the paper, which includes Refs. [14,17,21,23,29,36,37,49–70].

[49] W. Cochran, R. A. Crowley, G. Dolling, and M. M. Elcombe, Proc. R. Soc. London A **293**, 433 (1966).

[50] P. Fons, A. V. Kolobov, M. Krbal, J. Tominaga, K. S. Andrikopoulos, S. N. Yannopoulos, G. A. Voyiatzis, and T. Uruga, Phys. Rev. B **82**, 155209 (2010).

[51] E. Steigmeier and G. Harbeke, Solid State Commun. **8**, 1275 (1970).

[52] P. Bauer Pereira, I. Sergueev, S. Gorsse, J. Dadda, E. Müller, and R. P. Hermann, Phys. Status Solidi B **250**, 1300 (2013).

[53] R. Shaltaf, E. Durgun, J.-Y. Raty, P. Ghosez, and X. Gonze, Phys. Rev. B **78**, 205203 (2008).

[54] D. A. Broido, A. Ward, and N. Mingo, Phys. Rev. B **72**, 014308 (2005).

[55] R. Dalven, Infrared Phys. **9**, 141 (1969).

[56] B. Houston, R. E. Strakna, and H. S. Belson, J. Appl. Phys. **39**, 3913 (1968).

[57] P. K. Schelling and P. Keblinski, Phys. Rev. B **68**, 035425 (2003).

[58] T. Chatterji, C. M. N. Kumar, and U. D. Wdowik, Phys. Rev. B **91**, 054110 (2015).

[59] D. Yang, T. Chatterji, J. A. Schiemer, and M. A. Carpenter, Phys. Rev. B **93**, 144109 (2016).

[60] E. M. Levin, M. F. Besser, and R. Hanus, J. Appl. Phys. **114**, 083713 (2013).

[61] H. Wiedemeier and P. A. Siemers, Z. Anorg. Allg. Chem. **431**, 299 (1977).

[62] E. D. Devyatkova and I. A. Smirnov, Sov. Phys. Solid State, USSR **3**, 1666 (1962).

[63] A. A. El-Sharkawy, A. M. A. El-Azm, M. I. Kenawy, A. S. Hillal, and H. M. Abu-Basha, Int. J. Thermophys. **4**, 261 (1983).

[64] A. H. Romero, E. K. U. Gross, M. J. Verstraete, and O. Hellman, Phys. Rev. B **91**, 214310 (2015).

[65] P. Nath and K. L. Chopra, Phys. Rev. B **10**, 3412 (1974).

[66] P. B. Littlewood and V. Heine, J. Phys. C **12**, 4431 (1979).

[67] W. Zhong, R. D. King-Smith, and D. Vanderbilt, Phys. Rev. Lett. **72**, 3618 (1994).

[68] P. Ghosez, J. P. Michenaud, and X. Gonze, Phys. Rev. B **58**, 6224 (1998).

[69] U. V. Waghmare, N. A. Spaldin, H. C. Kandpal, and R. Seshadri, Phys. Rev. B **67**, 125111 (2003).

[70] M. S. Hybertsen and S. G. Louie, Phys. Rev. B **35**, 5585 (1987).

[71] A. Onodera, I. Sakamoto, Y. Fujii, N. Môri, and S. Sugai, Phys. Rev. B **56**, 7935 (1997).

[72] J. Goldak, C. S. Barrett, D. Innes, and W. Youdelis, J. Chem. Phys. **44**, 3323 (1966).

[73] M. P. Lee, M. Trigo, I. Savić, S. Fahy, E. D. Murray, C. Bray, J. Clark, T. Henighan, M. Kozina, M. Chollet, J. M. Glownia, M. C. Hoffman, D. Zhu, A. F. May, B. C. Sales, A. M. Lindenberg, P. Zalden, T. Sato, R. Merlin, and D. A. Reis, Nat. Commun. **7**, 12291 (2016).

[74] Y. Zhang, X. Ke, P. R. C. Kent, J. Yang, and C. Chen, Phys. Rev. Lett. **107**, 175503 (2011).

[75] T. Keiber, F. Bridges, and B. C. Sales, Phys. Rev. Lett. **111**, 095504 (2013).

[76] C. W. Li, O. Hellman, J. Ma, A. F. May, H. B. Cao, X. Chen, A. D. Christianson, G. Ehlers, D. J. Singh, B. C. Sales, and O. Delaire, Phys. Rev. Lett. **112**, 175501 (2014).

[77] Y. Chen, X. Ai, and C. A. Marianetti, Phys. Rev. Lett. **113**, 105501 (2014).

[78] E. S. Božin, C. D. Malliakas, P. Souvatzis, T. Proffen, N. A. Spaldin, M. G. Kanatzidis, and S. J. L. Billinge, Science **330**, 1660 (2010).

[79] K. M. O. Jensen, E. S. Božin, C. D. Malliakas, M. B. Stone, M. D. Lumsden, M. G. Kanatzidis, S. M. Shapiro, and S. J. L. Billinge, Phys. Rev. B **86**, 085313 (2012).

[80] S. Kastbjerg, N. Bindzus, M. Sndergaard, S. Johnsen, N. Lock, M. Christensen, M. Takata, M. A. Spackman, and B. B. Iversen, Adv. Funct. Mater. **23**, 5477 (2013).

[81] S. Christensen, N. Bindzus, M. Sist, M. Takata, and B. B. Iversen, Phys. Chem. Chem. Phys. **18**, 15874 (2016).

[82] K. M. Rabe and J. D. Joannopoulos, Phys. Rev. B **36**, 6631 (1987).

[83] T. Matsunaga, P. Fons, A. V. Kolobov, J. Tominaga, and N. Yamada, Appl. Phys. Lett. **99**, 231907 (2011).

[84] O. Hellman and I. A. Abrikosov, Phys. Rev. B **88**, 144301 (2013).

[85] M. Schlüter, G. Martinez, and M. L. Cohen, Phys. Rev. B **12**, 650 (1975).